

# Surface tension of the core-crust interface of neutron stars with global charge neutrality

Jorge A. Rueda,<sup>1,2</sup> Remo Ruffini,<sup>1,2,3</sup> Yuan-Bin Wu,<sup>1,2,3</sup> and She-Sheng Xue<sup>1,2</sup>

<sup>1</sup>*Dipartimento di Fisica and ICRA, Sapienza Università di Roma, P.le Aldo Moro 5, I-00185 Rome, Italy*

<sup>2</sup>*ICRANet, P.zza della Repubblica 10, I-65122 Pescara, Italy*

<sup>3</sup>*ICRANet, University of Nice-Sophia Antipolis, 28 Av. de Valrose, 06103 Nice Cedex 2, France*

It has been shown recently that taking into account strong, weak, electromagnetic, and gravitational interactions, and fulfilling the global charge neutrality of the system, a transition layer will happen between the core and crust of neutron stars, at the nuclear saturation density. We use relativistic mean field theory together with the Thomas-Fermi approximation to study the detailed structure of this transition layer and calculate its surface and Coulomb energy. We find that the surface tension is proportional to a power-law function of the baryon number density in the core bulk region. We also analyze the influence of the electron component and the gravitational field on the structure of the transition layer and the value of the surface tension to compare and contrast with known phenomenological results in nuclear physics. Based on the above results we study the instability against Bohr-Wheeler surface deformations in the case of neutron stars obeying global charge neutrality. Assuming the core-crust transition at nuclear density  $\rho_{core} \approx 2.7 \times 10^{14} \text{ g cm}^{-3}$ , we find that the instability sets the upper limit to the crust density,  $\rho_{crust}^{crit} \approx 1.2 \times 10^{14} \text{ g cm}^{-3}$ . This result implies a nonzero lower limit to the maximum electric field of the core-crust transition surface and makes inaccessible a limit of quasilocal charge neutrality in the limit  $\rho_{crust} = \rho_{core}$ . The general framework presented here can be also applied to study the stability of sharp phase transitions in hybrid stars as well as in strange stars, both bare and with outer crust. The results of this work open the way to a more general analysis of the stability of these transition surfaces, accounting for other effects such as gravitational binding, centrifugal repulsion, magnetic field induced by rotating electric field, and therefore magnetic dipole-dipole interactions.

PACS numbers: 26.60.-c, 97.60.Jd, 04.20.-q, 04.40.Dg

## I. INTRODUCTION

The relativistic mean field theory (RMFT) of nuclear matter and the Thomas-Fermi model have attracted great attention during the last few decades. The simplest relativistic model of nuclear matter that accounts for the saturation properties of symmetric nuclear matter includes one scalar field which gives the attractive long-range part of the nuclear force and one vector field which gives the repulsive short-range; these two meson fields interact with nucleons through Yukawa couplings. This so-called  $\sigma$ - $\omega$  model has been considered by Duerr [1], Miller and Green [2], and later by Walecka [3]. The physical understanding of this model has been very well studied the literature [4–11]. As recognized in Ref. [5], it is necessary to introduce additional isovector fields to obtain agreement with the empirical symmetry energy of nuclear matter at the saturation density. The model, containing Dirac nucleons together with a self-interacting scalar  $\sigma$  and a vector meson  $\omega$  as well as an isovector meson  $\rho$ , has been widely used to this end.

With a very limited number of parameters, the RMFT has been shown to be able to give a quantitative description of a variety of nuclear properties [12–14]. Recently, taking into account the electromagnetic and weak interactions, the RMFT with the Thomas-Fermi approximation has gained remarkable successes in understanding the inhomogeneous structures and properties of low-density nuclear matter which is realized in supernovae cores or in the crusts of neutron stars (see, e.g., Refs. [15–18]). The surface properties of nuclear matter such as surface tension and curvature energy play an important role in the description of these structures and also in other phenomena, for instance saddle-point configurations in nuclear fis-

sion, fragment distributions in heavy-ion collisions, and phase transition between different phases of nuclear matter.

The nuclear surface properties at saturation density have been analyzed for a long time in the semi-infinite nuclear matter model using RMFT [3] or effective field theory [19–21] with the Thomas-Fermi approximation or Hartree-Fock approximation [5, 22–30]. In the supranuclear regime realized in the interior of neutron stars, there is the possibility that phase transition occurs from hadronic to pion and kaon condensed phase as well as to quark matter phase (see, e.g., [31–33]). The surface tension of the transition layer between the hadronic and kaon condensed or quark matter phases has been calculated in the semi-infinite matter model, and the surface tension plays an important role in the structure of the phase transition region [34, 35]. In the low-density (density smaller than the saturation density) case, as pointed out in [36], the shape of constituent nuclei is expected to change from spherical droplet to the so-called nuclear pasta structures such as cylindrical rod, slab, cylindrical tube, and spherical bubble. The surface tensions of nuclear pasta structures have been investigated and it has been pointed out that the pasta phase strongly depends on the value of the surface tension [15, 16, 18].

The importance of the extension of the Thomas-Fermi approximation to general relativistic systems such as neutron stars was emphasized in Ref. [37]. We showed there that the traditionally imposed condition of local charge neutrality is not consistent with the field equations and microphysical equilibrium for a system of neutrons, protons, and electrons in  $\beta$  equilibrium and obeying relativistic quantum statistics. Thus, only the condition of global but not local charge neutrality can be imposed. This leads to the appearance of gravito-

polarization in the cores of neutron stars. The generalization of such a work to the case where the strong interactions between nucleons are accounted for was presented in [38]. Both the Thomas-Fermi approximation and RMFT were used. It was shown that the Einstein-Maxwell-Thomas-Fermi (EMTF) system of equations within RMFT supersede the traditional Tolman-Oppenheimer-Volkoff (TOV) [39, 40] equations used for the construction of neutron star configurations.

Realistic neutron star configurations including all the interactions between particles and the presence of a crust below nuclear density, were constructed in Ref. [41] by solving numerically the EMTF equations fulfilling the condition of global charge neutrality. As pointed out in [41], the self-consistent solution of these new equations of equilibrium leads to the existence of a transition layer between the core and the crust of the star. This is markedly different from the neutron star structure obtained from the solution of the TOV equations imposing local charge neutrality (see e.g., [42]), leading to a new mass-radius ( $M$ - $R$ ) relation of neutron stars. The core-crust transition layer in our configurations occurs near the nuclear saturation density  $\rho_{nucl}$ . The core (bulk region) inside this transition layer is a hadronic phase, and the crust outside this transition is composed of the nuclei lattice and the ocean of relativistic degenerate electrons and possibly neutrons at densities below nuclear saturation and larger than the estimated neutron drip value  $\sim 4.3 \times 10^{11} \text{ g cm}^{-3}$ . Inside the transition region a very strong electric field which is overwhelming is the critical value  $E_c = m_e^2 c^3 / (e\hbar)$  for vacuum breakdown is developed, where  $m_e$  is the electron rest mass. The  $e^+e^-$  pair creation from vacuum is, however, forbidden in the system due to the Pauli blocking of degenerate electrons.

In this article we study the surface properties of this transition layer formed near the nuclear saturation density. We calculate all the contributions to the surface tension as well as the electrostatic energy stored in this core-crust layer. We analyze the stability of these systems under the Bohr-Wheeler fission mechanism [43]. We analyze the role of the influence of the gravitational field on the structure of the transition layer and the surface tension. We also compare and contrast the surface energy of these neutron stars with the phenomenological results in nuclear physics.

The article is organized as follows. In Sec. II, we present the general formulation of the surface tension as well as the Coulomb energy for this core-crust transition layer. We formulate in Sec. II A the relativistic equations for a system of neutrons, protons, and electrons fulfilling the strong, electromagnetic, and gravitational interactions as well as  $\beta$  equilibrium. In Sec. II B, we use the semi-infinite matter model [44] to formulate the equations governing the surface tension for the transition layer of this system when the electron density is nearly equal to the proton density in the core bulk region. In Sec. III, we study the surface tension and the Coulomb energy, neglecting the presence of the crust and the gravitational interaction. We calculate the surface structure and solve these equations to obtain the surface tension and the Coulomb energy at the nuclear saturation density in Sec. III A. Then we study in Sec. III B the dependence of the surface tension and the Coulomb energy on the baryon number density.

In Sec. IV, we study the influence of fermion densities in the outside region (crust) on the surface tension and the Coulomb energy. In Sec. V, we study the structure and the surface tension as well as the Coulomb energy for the core-crust transition region in the presence of the gravitational field. We finally summarize and conclude in Sec. VI. We use units with  $\hbar = c = 1$  throughout the article.

## II. RELATIVISTIC EQUATIONS OF MOTION AND SURFACE TENSION

### A. Relativistic equations of motion

As described in Ref. [41], the system we consider is composed of degenerate neutrons, protons, and electrons fulfilling global charge neutrality and  $\beta$  equilibrium. We include the strong, electromagnetic, weak, and gravitational interactions. To describe the nuclear interactions, we employ the RMFT with the Thomas-Fermi approximation. We adopt the phenomenological nuclear model of Boguta and Bodmer [5].

We introduce the nonrotating spherically symmetric spacetime metric

$$ds^2 = e^{\nu(r)} dt^2 - e^{\lambda(r)} dr^2 - r^2 d\theta^2 - r^2 \sin^2 \theta d\phi^2, \quad (1)$$

where the  $\nu(r)$  and  $\lambda(r)$  are only functions of the radial coordinate  $r$ .

Within the Thomas-Fermi approximation and mean-field approximation, we can obtain the full system of general relativistic equations. A detailed description of this model can be found in Ref. [41]. We are here interested in the core-crust transition layer, which as we have shown happens in a tiny region [41] with a characteristic length scale  $\sim \lambda_e = \hbar / (m_e c) \sim 100 \text{ fm}$ . Correspondingly, the metric functions are essentially constant in this region. Thus in the core-crust transition layer the system of equations can be written as

$$\frac{d^2 V}{dr^2} + \frac{2}{r} \frac{dV}{dr} = -4\pi e e^{\nu_{core}/2} e^{\lambda_{core}} (n_p - n_e), \quad (2)$$

$$\frac{d^2 \sigma}{dr^2} + \frac{2}{r} \frac{d\sigma}{dr} = e^{\lambda_{core}} [\partial_\sigma U(\sigma) + g_s n_s], \quad (3)$$

$$\frac{d^2 \omega}{dr^2} + \frac{2}{r} \frac{d\omega}{dr} = -e^{\lambda_{core}} (g_\omega J_0^\omega - m_\omega^2 \omega), \quad (4)$$

$$\frac{d^2 \rho}{dr^2} + \frac{2}{r} \frac{d\rho}{dr} = -e^{\lambda_{core}} (g_\rho J_0^\rho - m_\rho^2 \rho), \quad (5)$$

$$E_e^F = e^{\nu_{core}/2} \mu_e - eV = \text{constant}, \quad (6)$$

$$E_p^F = e^{\nu_{core}/2} \mu_p + g_\omega \omega + g_\rho \rho + eV = \text{constant}, \quad (7)$$

$$E_n^F = e^{\nu_{core}/2} \mu_n + g_\omega \omega - g_\rho \rho = \text{constant}, \quad (8)$$

where the notation  $\omega_0 \equiv \omega$ ,  $\rho_0 \equiv \rho$ , and  $A_0 \equiv V$  for the time components of the meson fields have been introduced. Here  $\mu_i = \sqrt{(P_i^F)^2 + \tilde{m}_i^2}$  and  $n_i = (P_i^F)^3 / (3\pi^2)$  are the free chemical potential and number density of the  $i$ -fermion species with Fermi momentum  $P_i^F$ . The particle effective masses are  $\tilde{m}_N = m_N + g_s \sigma$  and  $\tilde{m}_e = m_e$ , where  $m_i$  stands for the

rest mass of each  $i$ -fermion species.  $e^{v_{core}} \equiv e^{v(R_{core})}$  and  $e^{\lambda_{core}} \equiv e^{\lambda(R_{core})}$  are the metric functions evaluated at the core radius  $R_{core}$ .  $g_s$ ,  $g_\omega$ , and  $g_\rho$  are the coupling constants of the  $\sigma$ ,  $\omega$  and  $\rho$  fields,  $e$  is the fundamental electric charge, and  $m_\omega$ , and  $m_\rho$  are the masses of  $\omega$  and  $\rho$ . The scalar self-interaction potential is

$$U(\sigma) = \frac{1}{2}m_\sigma^2\sigma^2 + \frac{1}{3}g_2\sigma^3 + \frac{1}{4}g_3\sigma^4, \quad (9)$$

with the  $\sigma$  meson mass  $m_\sigma$  and the third- and fourth- order constants of the self-scalar interactions  $g_2$  and  $g_3$ .

The generalized Fermi energies of electrons, protons, and neutrons,  $E_e^F$ ,  $E_p^F$ , and  $E_n^F$  (so-called the Klein potentials [38]), are linked by the  $\beta$  equilibrium [45] of protons, neutrons, and electrons,

$$E_n^F = E_p^F + E_e^F. \quad (10)$$

The scalar density  $n_s$  is given by the expectation value

$$n_s = \langle \bar{\psi}_N \psi_N \rangle = \frac{2}{(2\pi)^3} \sum_{i=n,p} \int_0^{p_i^F} d^3k \frac{\tilde{m}_N}{\varepsilon_i(k)}, \quad (11)$$

where  $\varepsilon_i(k) = \sqrt{k^2 + \tilde{m}_i^2}$  is the single-particle energy, and  $\psi_N$  is the nucleon isospin doublet. In the static case, the nonvanishing components of the currents are

$$J_0^{ch} = e^{v_{core}/2}(n_p - n_e), \quad (12)$$

$$J_0^\omega = e^{v_{core}/2}(n_n + n_p), \quad (13)$$

$$J_0^\rho = e^{v_{core}/2}(n_p - n_n), \quad (14)$$

here  $n_b = n_p + n_n$  is the baryon number density.

The parameters of the nuclear model, namely the coupling constants  $g_s$ ,  $g_\omega$ , and  $g_\rho$ , the meson masses  $m_\sigma$ ,  $m_\omega$ , and  $m_\rho$ , and the self-scalar interaction constants  $g_2$  and  $g_3$  are fixed by fitting nuclear experimental data. We here use the parameters of the NL3 parametrization [46], shown in Table I.

$m_\sigma$ (MeV)	508.194	$g_\omega$	12.8680
$m_\omega$ (MeV)	782.501	$g_\rho$	4.4740
$m_\rho$ (MeV)	763.000	$g_2$ (fm <sup>-1</sup> )	-10.4310
$g_s$	10.2170	$g_3$	-28.8850

TABLE I: The parameters of the nuclear model from NL3.

Since the equation of state (EOS) obtained from the RMFT is very stiff (see, e.g., [42]), it is natural to evaluate its consequences on causality. In order to do this, we compute the material sound velocity,  $v_s^2 = d\varepsilon/d\mathcal{P}$ , as a function of the central density  $\rho(0) = \varepsilon(0)/c^2$  of the configuration, where  $\varepsilon = T_0^0$  and  $\mathcal{P} = -T_1^1$  are total energy-density and pressure of the system,  $T_0^0$  and  $T_1^1$  being the 0-0 and 1-1 components of the energy-momentum tensor [41].

The result is shown in Fig. 1. We recall that the instability against gravitational collapse sets in at the turning point

in the  $M$ - $\rho(0)$  diagram, namely at the first maximum in the sequence of equilibrium configurations with increasing central density, namely  $dM/d\rho(0) = 0$ . Such a point gives us the maximum stable mass  $M_{max}$ , which for the present EOS is  $M_{max} \approx 2.67 M_\odot$ , where  $M_\odot$  is the solar mass. It can be seen from Fig. 1 that  $v_s < c$ , where  $c$  is the velocity of light, at any density in the entire range of  $\rho(0)$  of the stable configurations, and therefore the used EOS does not violate causality.

It is important to mention that the above critical point for the gravitational collapse does not coincide with the point of backbending of the  $M$ - $R$  relation (see, e.g., Figs. 6 and 14 in [41]). Therefore the backbending in the  $M$ - $R$  diagram does not indicate any sort of instability.

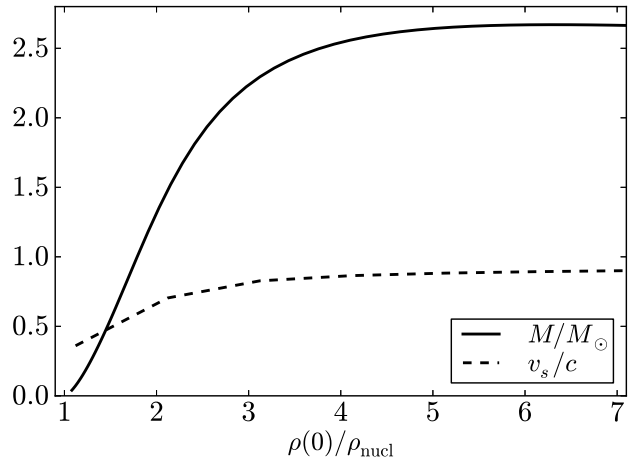


FIG. 1: The dependence of the total mass  $M$  of the star and the material sound velocity  $v_s$  on the central density  $\rho(0)$  of the configuration.

## B. Surface tension for semi-infinite matter

As shown in [41], in the bulk hadronic phase of neutron star cores, the charge separation is very small, so the electron density  $n_{eb}$  is nearly equal to the proton density  $n_{pb}$ . In addition, the core-crust transition layer has a characteristic length scale of the order of the electron Compton wavelength; this is very small compared to the radius of neutron stars. So it is a good approximation to use the semi-infinite matter model to construct the surface tension for the system we consider here. We construct the surface tension for the transition layer of this system following the method of Baym, Bethe, and Pethick (BBP) [44].

In the semi-infinite matter model, one assumes a plane surface with small thickness compared with the bulk region size separating two semi-infinite regions, represented here by the inside core bulk and the outside crust. The number density of the  $i$ -fermion species ( $i = n, p, e$ )  $n_i(r)$  approaches the bulk density of the  $i$ -fermion species  $n_{ib}$  as the position  $\bar{r} \equiv (r - R_{core}) \rightarrow -\infty$ , and approaches the density in the outside region of the  $i$ -fermion species  $n_{io}$  as the  $\bar{r} \rightarrow +\infty$ . To construct the surface tension, one imagines a reference system with a sharp surface at  $\bar{r} = a_i$  at which fermion densities and

meson fields fall discontinuously from the core bulk region to the outside crust region. Following Ref. [44], the location of the reference surface for the  $i$ -fermion species is defined by the condition that the reference system has the same number of the  $i$ -fermion species as the original system. Following the definition of fermion number in the curved spacetime, Eq. (1) (see, e.g., [47]), the  $i$ -fermion species number  $N_i$  is given by

$$N_i = 4\pi \int e^{\lambda/2} r^2 n_i(r) dr. \quad (15)$$

Since the metric functions are constant in the surface region we consider as described in Sec. II A, and the size of the surface region is very small compared to the radius of neutron stars, we can treat  $e^{\lambda/2} r^2$  as a constant in the integral, the location of the reference surface for the  $i$ -fermion species is given by

$$\int_{-\infty}^{a_i} d\bar{r} [n_i(\bar{r}) - n_{ib}] + \int_{a_i}^{\infty} dr [n_i(\bar{r}) - n_{io}] = 0, \quad i = n, p, e. \quad (16)$$

Applying the definition of the reference surface in Eq. (16) to the neutron, proton, and electron distributions yields slightly different reference surfaces.

Similar to the definition of the reference surface for the fermion, we define the location of the reference surfaces for meson fields by

$$\int_{-\infty}^{a_i} d\bar{r} [F_i(\bar{r}) - F_{ib}] + \int_{a_i}^{\infty} d\bar{r} [F_i(\bar{r}) - F_{io}] = 0, \quad i = \sigma, \omega, \rho, \quad (17)$$

where  $F_i(\bar{r})$  is the time component of the  $i$ -meson field,  $F_{ib}$  is the time component of the  $i$ -meson field in the bulk region, and  $F_{io}$  is the time component of the  $i$ -meson field in the outside region.

The energy associated to the density  $\varepsilon(r) = T_0^0$ , where  $T_\beta^\alpha$  is the energy-momentum tensor of the system, can be calculated in the spherically symmetric metric by (see, e.g., [47])

$$E_t = 4\pi \int e^{(\nu+\lambda)/2} r^2 \varepsilon(r) dr. \quad (18)$$

Thus, the total surface tension can be written as the sum of three contributions,

$$\sigma_t = \sigma_N + \sigma_e + \sigma_C, \quad (19)$$

where we have introduced the nuclear surface tension following the method of BBP [44],

$$\begin{aligned} \sigma_N = & \sum_{i=n,p,\sigma,\omega,\rho} e^{(\nu_{core}+\lambda_{core})/2} \left\{ \int_{-\infty}^{a_i} [\varepsilon_i(\bar{r}) - \varepsilon_{ib}] d\bar{r} \right. \\ & \left. + \int_{a_i}^{\infty} [\varepsilon_i(\bar{r}) - \varepsilon_{io}] d\bar{r} \right\}, \end{aligned} \quad (20)$$

the electron surface tension

$$\begin{aligned} \sigma_e = & e^{(\nu_{core}+\lambda_{core})/2} \left\{ \int_{-\infty}^{a_e} [\varepsilon_e(\bar{r}) - \varepsilon_{eb}] d\bar{r} \right. \\ & \left. + \int_{a_e}^{\infty} [\varepsilon_e(\bar{r}) - \varepsilon_{eo}] d\bar{r} \right\}, \end{aligned} \quad (21)$$

and the surface tension for the electric field as

$$\sigma_C = e^{(\nu_{core}+\lambda_{core})/2} \int_{-\infty}^{\infty} \varepsilon_E(\bar{r}) d\bar{r}. \quad (22)$$

with  $\varepsilon_i(\bar{r})$  the energy density of the  $i$  species of fermion or meson fields,  $\varepsilon_{ib}$  is the energy density of the  $i$  species of fermion or meson fields in the bulk region,  $\varepsilon_{io}$  is the energy density of the  $i$  species of fermion or meson fields in the outside region, and  $\varepsilon_E(\bar{r}) = E^2/(8\pi)$  is the electrostatic energy density. In the curved spacetime equation (1), the electric field is given by (see, e.g., [41])

$$E = e^{-(\lambda_{core}+\nu_{core})/2} \frac{dV}{dr}. \quad (23)$$

It is important to clarify how the values of  $n_{io}$  and  $\varepsilon_{io}$  are obtained. As we showed in Ref. [41], the Einstein-Maxwell-Thomas-Fermi equations have to be solved under the constraint of global charge neutrality and not local charge neutrality, as in the traditional TOV-like treatment. In the latter locally neutral configurations, the continuity of total pressure leads to neutron stars with a crust starting from nuclear density, where the clusterization of nucleons starts to be preferred over the homogenous phase of the core, all the way up to low densities in the surface. The region between nuclear density and the neutron-drip density,  $\rho_{drip} \approx 4.3 \times 10^{11} \text{ g cm}^{-3}$ , is called the *inner crust*, and at lower densities,  $\rho < \rho_{drip}$ , the *outer crust*. In this case the continuity of the pressure does not ensure the continuity of the particle generalized chemical potentials. For electrons it implies an inconsistency since the mismatching of the electrochemical potential implies the existence of a Coulomb potential energy, not accounted for in such a treatment (see, e.g., Ref. [37]).

In the globally neutral case, there is a different core-crust boundary problem: the generalized fermion chemical potentials have to match, at the end of the core-crust transition boundary layer, their corresponding values at the base of the crust (outside region); i.e., they must satisfy a condition of continuity (see Ref. [41] for details). It implies that the values of  $n_{io}$  and  $\varepsilon_{io}$  depend on the density at the base of the crust under consideration.

We first consider below in Section III the surface tension of the system neglecting the presence of the crust. Then, the more realistic case of a neutron star with a crust is considered in Section IV. Configurations with only outer crust as well as configurations with both inner and outer crust are studied.

Turning to the Coulomb energy, it is important to remark that, owing to the small charge separation present in the system in the core bulk region, we can assume that the electric field only exists in the transition layer surface. Thus we can consider the electrostatic energy as a surface property of the system, hence contributing to the surface energy. This is a major difference between the present system and an ordinary nucleus where the electrostatic energy is a volume property.

The relation between the surface energy and Coulomb energy is very important for a nucleus. As shown by Bohr and Wheeler [43] when the condition

$$E_{coul} > 2E_{sur} \quad (24)$$



is satisfied, the nucleus becomes unstable against nuclear fission; here  $E_{coul}$  is the Coulomb energy of the nucleus and  $E_{sur}$  is the surface energy of the nucleus. It is important to recall that the idealized picture of the deformed nucleus of Bohr and Wheeler is represented by two positively charged spheres joined by a nuclear attraction neck. It is thus the interplay of the Coulomb and nuclear surface energies that determines the lower energy state. Following this argument one could think that, since we are treating here a globally neutral system, such an instability mechanism is absent. However, the condition (24) can be also obtained by requesting that a uniformly charged spheroid, constructed from an axially symmetric deformation at constant volume of a uniformly charged sphere, be energetically favorable. From a careful look at the derivation of Eq. (24)—see, e.g., Ref.[48]—it can be seen that this result follows from the fact that Coulomb energy of the unperturbed system (the sphere) depends on the radius as  $E_{coul} \propto R^{-1}$ . Such an inverse radius dependence holds also in the case of a uniformly charged shell, and also in the case of the globally neutral massive nuclear density cores studied in Refs. [49, 50], which fully reflect the properties of the system studied in this work. We then expect that the Bohr-Wheeler condition of instability against fission given by Eq. (24) applies also to our system. Clearly such a condition is obtained keeping the system at nuclear density and neglecting the extra binding effect of gravity.

In thermodynamics, the surface tension is related to the mechanical work needed to increase a surface area [51],

$$dW = \sigma dS, \quad (25)$$

here  $\sigma$  is the surface tension,  $dS$  is the variation of the surface area, and  $dW$  is the mechanical work needed to increase the surface area of the system. In this point of view, a system with a positive surface tension has an attractive nature, and a system with a negative surface tension has a repulsive nature.

Equations (19)-(22) show that the surface tension mainly depends on the fermion density and meson field profiles and the energy densities of fermions and meson fields. The energy density of the  $i$ -fermion species is given by

$$\varepsilon_i(\bar{r}) = \frac{1}{8\pi^2} \left\{ P_i^F \sqrt{(P_i^F)^2 + \tilde{m}_i^2} [2(P_i^F)^2 + \tilde{m}_i^2] - \tilde{m}^4 \ln \frac{P_i^F + \sqrt{(P_i^F)^2 + \tilde{m}_i^2}}{\tilde{m}_i} \right\}, \quad (26)$$

and the energy densities of the meson fields are (see, e.g., [47])

$$\varepsilon_\sigma(\bar{r}) = \frac{1}{2} e^{-\lambda_{core}} \left( \frac{d\sigma}{d\bar{r}} \right)^2 + U(\sigma), \quad (27)$$

$$\varepsilon_\omega(\bar{r}) = \frac{1}{2} e^{-(\lambda_{core} + \nu_{core})} \left( \frac{d\omega}{d\bar{r}} \right)^2 + \frac{1}{2} e^{-\nu_{core}} m_\omega^2 \omega^2, \quad (28)$$

$$\varepsilon_\rho(\bar{r}) = \frac{1}{2} e^{-(\lambda_{core} + \nu_{core})} \left( \frac{d\rho}{d\bar{r}} \right)^2 + \frac{1}{2} e^{-\nu_{core}} m_\rho^2 \rho^2, \quad (29)$$

$$\varepsilon_E(\bar{r}) = e^{-(\lambda_{core} + \nu_{core})} \frac{1}{8\pi} \left( \frac{dV}{d\bar{r}} \right)^2. \quad (30)$$

We can solve Eqs. (2)-(8) together with the  $\beta$  equilibrium (10) to obtain the fermion density and meson field profiles. Following the similar method in Ref. [41], this system of equations can be numerically solved with appropriate conditions and approximations:

- set a value for baryon number density of the bulk region  $n_{bb} = n_{nb} + n_{pb}$ ;
- in the bulk core region the electron density  $n_{eb}$  is nearly equal to the proton density  $n_{pb}$ , i.e.  $n_{pb} \simeq n_{eb}$ ;
- set values for  $e^{\nu_{core}}$  and  $e^{-\lambda_{core}}$ ;
- the values of  $n_{i0}$  have to match their corresponding values at the edge of the crust.

### III. SURFACE TENSION NEGLECTING THE PRESENCE OF A CRUST

#### A. Surface tension at nuclear saturation density

We first consider in this section the surface properties of this transition layer neglecting the presence of the crust and the gravitational interaction, i.e.,  $n_{i0} = 0$  and  $(e^{\nu_{core}}, e^{-\lambda_{core}}) \rightarrow 1$ , as a special case to gain some physical insight into this transition layer. Also we assume here the baryon number density of the bulk region to be the nuclear saturation density,  $n_{bb} = n_{nb} + n_{pb} = n_{nucl} = 0.16 \text{ fm}^{-3}$ . The solution of Eqs. (2)-(8) in this case is shown in Fig. 2. Since the fermion densities tend to be zero in the outside region, the thickness of the surface region for electrons should be infinite. However, we just show the results up to a very small electron density here, due to the plot scale and the accuracy of the numerical calculation. As shown in Fig. 2, before a sharp decrease of the proton and neutron densities, there is a bump on the proton density profile due to Coulomb repulsion while the electron density profile decreases.

Using the definitions in Eqs. (19)-(22), we can calculate the surface tensions for this transition layer. The results are shown in Table II. In order to study the effect of the  $\rho$  meson, we also show in Table II the surface tensions in the case when the  $\rho$  meson is not present. The presence of  $\rho$  decreases the total surface tension  $\sigma_t$  but increases the Coulomb energy, and so  $\sigma_C$ . We can see that the difference of the surface tension for nucleons,  $\sigma_N$ , in the presence and absence of the  $\rho$  meson is relatively small with respect to the changes on the electron component and the electric field. We can explain this small difference from the fact that, although the  $\rho$  meson increases the proton to neutron density ratio, in neutron stars the  $\beta$  equilibrium in the presence of degenerate electrons leads to a high isospin asymmetry  $1 - 2Z/A \approx 1$ , hence the system is still dominated by the neutron component, as we show below.

It is interesting to compare the above results with the nuclear surface tension in the literature. The nuclear surface properties at saturation density have been widely discussed in relativistic and nonrelativistic models. The value of the nuclear surface tension in the literature is around  $\sigma_L \sim 1 \text{ MeV}$

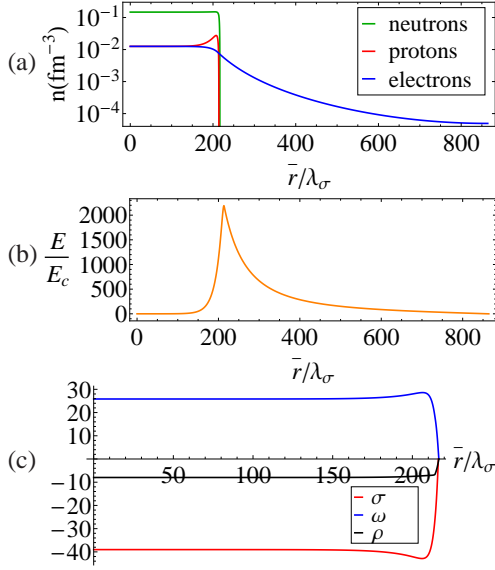


FIG. 2: (Color online) (a) Fermion density profiles in units of  $\text{fm}^{-3}$ . (b) Electric field in units of the critical field  $E_c = m_e^2 c^3 / (e\hbar)$ . (c) Meson fields  $\sigma$ ,  $\omega$ , and  $\rho$  in units of MeV. Here  $n_{bb} = n_{nucl}$ ,  $n_{i0} = 0$ , and  $(e^{V_{core}}, e^{-\lambda_{core}}) \rightarrow 1$ .  $\lambda_\sigma = \hbar / (m_\sigma c) \sim 0.4$  fm is the Compton wavelength of the  $\sigma$  meson.

	$\sigma_t$	$\sigma_N$	$\sigma_e$	$\sigma_C$
$\sigma \ \omega$	6.28	7.07	-1.72	0.92
$\sigma \ \omega \ \rho$	3.10	7.30	-8.34	4.14

TABLE II: Total and specific surface tensions in  $\text{MeV fm}^{-2}$  of the transition layer with and without the presence of the  $\rho$  meson. We set here  $n_{bb} = n_{nucl}$ ,  $n_{i0} = 0$ , and  $(e^{V_{core}}, e^{-\lambda_{core}}) \rightarrow 1$ .

$\text{fm}^{-2}$ ; see, e.g., Refs. [27, 28]. The difference between our result in Table II and  $\sigma_L$  is mainly due to the fact that the presence of degenerate electrons changes the proton and neutron density profiles and also leads to a high isospin asymmetry of our system as a byproduct of the  $\beta$ -equilibrium condition. Especially, there is a bump on the density profiles in our system, which would not appear in the case of normal nuclear matter. Further discussions about this point is given below; see also Table III.

In order to understand where the surface tension comes from, we calculate the contribution of each fermion and meson field to the surface tension as

$$\sigma_n = \int_{-\infty}^{a_n} [\epsilon_n(z) - \epsilon_{nb}] dz + \int_{a_n}^{\infty} [\epsilon_n(z) - \epsilon_{no}] dz, \quad (31)$$

$$\sigma_p = \int_{-\infty}^{a_p} [\epsilon_p(z) - \epsilon_{pb}] dz + \int_{a_p}^{\infty} [\epsilon_p(z) - \epsilon_{po}] dz, \quad (32)$$

$$\sigma_e = \int_{-\infty}^{a_e} [\epsilon_e(z) - \epsilon_{eb}] dz + \int_{a_e}^{\infty} [\epsilon_e(z) - \epsilon_{eo}] dz, \quad (33)$$

$$\sigma_\sigma = \int_{-\infty}^{a_\sigma} [\epsilon_\sigma(z) - \epsilon_{\sigma b}] dz + \int_{a_\sigma}^{\infty} [\epsilon_\sigma(z) - \epsilon_{\sigma o}] dz, \quad (34)$$

$$\sigma_\omega = \int_{-\infty}^{a_\omega} [\epsilon_\omega(z) - \epsilon_{\omega b}] dz + \int_{a_\omega}^{\infty} [\epsilon_\omega(z) - \epsilon_{\omega o}] dz, \quad (35)$$

$$\sigma_\rho = \int_{-\infty}^{a_\rho} [\epsilon_\rho(z) - \epsilon_{\rho b}] dz + \int_{a_\rho}^{\infty} [\epsilon_\rho(z) - \epsilon_{\rho o}] dz. \quad (36)$$

The results are shown in Table III. For the sake of comparison we also show the results in the case of ordinary nuclear matter, namely for a system without the presence of electrons. As shown in Ref. [41], comparing to the profiles in the case without the presence of the  $\rho$  meson, the presence of the  $\rho$  meson leads to larger proton and electron densities, and a larger bump of proton density happens. This effect is felt indirectly by neutrons (although much less strongly), due to the coupled nature of the system of equations (2)-(8). There is no such bump of the profiles in the case of normal nuclear matter. Comparing the results of the three cases in Table III, the effect of the bump of proton density on the surface tension is significant. The bump on the profiles decreases the value of the surface tension for fermions and increases the one for bosons. These results provide evidence of large effect of electromagnetic interaction and electrons on the proton and neutron density profiles, and therefore on the global value of the surface energy of the system. It can be seen from Table III that we obtain a surface tension of ordinary nuclear matter at saturation density (see the last line),  $\sigma_N \approx 1.7$   $\text{MeV fm}^{-2}$ . In our calculation,  $n_n$  is slightly larger than  $n_p$  according to the  $\beta$  equilibrium. This result is in agreement with the nuclear surface tension with a small neutron excess, e.g., in Ref. [27].

	$\sigma_n$	$\sigma_p$	$\sigma_e$	$\sigma_\sigma$	$\sigma_\omega$	$\sigma_\rho$
$n \ p \ e \ \sigma \ \omega$	3.54	-0.36	-1.72	3.16	0.73	
$n \ p \ e \ \sigma \ \omega \ \rho$	-27.35	-5.19	-8.34	22.20	19.93	-2.28
$n \ p \ \sigma \ \omega \ \rho$	19.43	12.23		-16.08	-13.83	-0.04

TABLE III: Contribution of each fermion and meson field to the surface tension, in  $\text{MeV fm}^{-2}$ . First row: the transition layer without the presence of the  $\rho$  meson. Second row: the transition layer with the presence of the  $\rho$  meson. Third row: normal nuclear matter (without the presence of electrons). We set  $n_{bb} = n_{nucl}$ ,  $n_{i0} = 0$ , and  $(e^{V_{core}}, e^{-\lambda_{core}}) \rightarrow 1$ .

## B. Influence of baryon number density on the surface tension

In order to study the dependence of the surface tension on the baryon number density, we calculate the surface tensions for different  $n_{bb}$  following the similar procedure in Sec. III A. The results are shown in Fig. 3. Here the presence of the crust and the gravitational interaction is neglected, i.e.,  $n_{i0} = 0$  and  $(e^{V_{core}}, e^{-\lambda_{core}}) \rightarrow 1$ . From the results, the total surface tension can be fitted by

$$\sigma_{t,fit} = 1.05 + 2.02 \left( \frac{n_{bb}}{n_{nucl}} \right)^{3.33} \quad (\text{MeV fm}^{-2}), \quad (37)$$

the surface tension for the electric field can be fitted by

$$\sigma_{C,fit} = -0.37 + 4.50 \left( \frac{n_{bb}}{n_{nucl}} \right)^2 \text{ (MeV fm}^{-2}\text{)}, \quad (38)$$

and the surface tension for nucleons can be fitted by

$$\sigma_{N,fit} = 0.95 + 6.33 \left( \frac{n_{bb}}{n_{nucl}} \right)^{2.91} \text{ (MeV fm}^{-2}\text{)}. \quad (39)$$

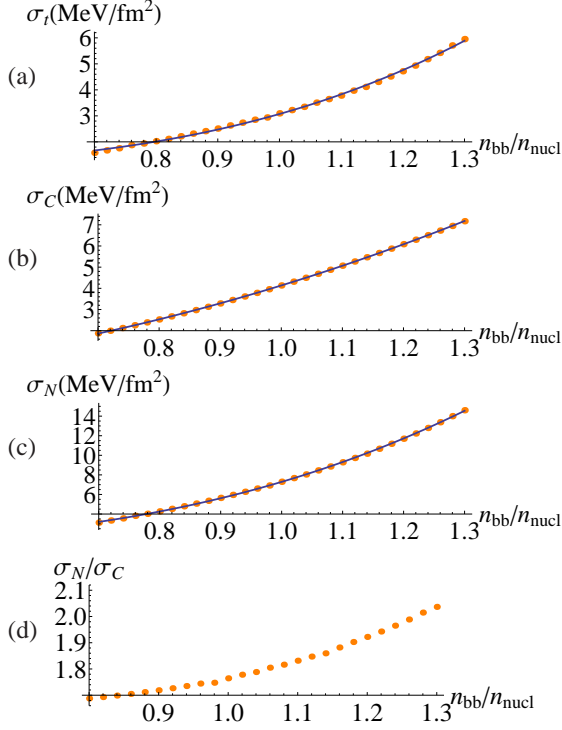


FIG. 3: (Color online) The dependence of the surface tension of the transition layer on the baryon number density in the bulk region. Here  $n_{i0} = 0$  and  $(e^{\nu_{core}}, e^{-\lambda_{core}}) \rightarrow 1$ . (a) The total surface tension  $\sigma_r$ , compared with the fit given in Eq. (37). (b) Surface tension for the electric field  $\sigma_C$ , compared with the fit given in Eq. (38). (c) Surface tension for nucleons  $\sigma_N$ , compared with the fit given in Eq. (39). (d) Ratio of the surface tension for nucleons and the surface tension for the electric field  $\sigma_N/\sigma_C$ .

As shown by BBP in [44], the phenomenological surface tension for nucleons within the Thomas-Fermi approximation can be written as

$$\sigma_{sur}^{BBP} = B(W_o - W_i)^{\frac{1}{2}}(n_i - n_o)^{\frac{3}{2}}, \quad (40)$$

where  $B$  is a constant,  $W_o$  and  $W_i$  are the binding energies per nucleon in the outside and inside bulk regions,  $n_o$  and  $n_i$  are the nucleon number densities in the outside and inside bulk regions. In the case of this section, we set the fermion densities and meson fields to be zero in the outside region, i.e.,  $n_o = W_o = 0$ . Since the fractional concentration of protons in the system we consider here is small, the binding energy per

nucleon is [44]

$$\begin{aligned} W(k, x) &= W(k, 0) + f(x) \\ &\approx 19.74k^2 - k^3 \frac{40.4 - 1.088k^3}{1 + 2.545k} + f(x), \end{aligned} \quad (41)$$

where  $k$  is defined by  $n = 2k^3/(3\pi^2)$ , with  $n$  the nucleon number density, and  $x$  is the fractional concentration of protons. The function  $f(x)$  is a small correction to  $W(k, 0)$  since  $x$  is small in our system. From Eq. (41), one can estimate that the leading term in the binding energy  $W_i$  is the kinetic term, proportional to  $k^2$ , i.e.,  $W_i \propto k^2 \propto n_{bb}^{2/3}$ . Thus one can estimate that  $\sigma_{sur}^{BBP} \propto n_{bb}^{11/6}$  in the BBP phenomenological result [44], where the effect of electromagnetic interaction on the profile of fermion density is neglected. This BBP phenomenological result is different from our result in Eq. (39). This is due to the fact that the electromagnetic interaction and the presence of electrons change the proton and neutron density profiles.

For  $\sigma_C$ , as shown in Eq. (38) the surface tension for the electric field is proportional to the square of the baryon number density. This result can be understood as follows. The Thomas-Fermi equilibrium condition for electrons given by Eq. (6) tells us that the Coulomb potential in the bulk core is proportional to the bulk electron chemical potential, so  $V_b \propto \mu_{eb}$ , and since the electrons are ultrarelativistic at these densities we have  $V_b \propto P_{eb}^F \propto n_{eb}^{1/3}$ . The thickness of the layer is of order  $\Delta r \sim n_{eb}^{-1/3}$  and so the electric field scales as  $E \sim -\Delta V/\Delta r \sim V_b/\Delta r \propto n_{eb}^{2/3}$ . Thus the contribution of the Coulomb energy to the surface tension satisfies  $\sigma_C \propto E^2 \Delta r \propto n_{eb}$  and since in the bulk core we have  $n_{eb} \simeq n_{pb}$  we obtain  $\sigma_C \propto n_{eb} = y n_{bb}$ , where  $y = n_{pb}/n_{bb}$  is the proton fraction in the bulk region. In neutron stars the  $\beta$  equilibrium between neutrons, protons, and electrons leads to a highly nuclear isospin asymmetry ( $y \ll 1$ ), and since the nucleons are approximately nonrelativistic and the electrons ultrarelativistic around nuclear saturation density, it can be estimated from Eq. (10) that the proton fraction is proportional to the baryon density, i.e.,  $y \propto n_{bb}$ , and therefore we finally obtain our final result  $\sigma_C \propto n_{bb}^2$ .

In Fig. 3 we show also the nuclear-to-Coulomb surface tension ratio  $\sigma_N/\sigma_C$ . We find that this ratio is larger than unity for all baryon number densities we considered. This would in principle imply that the system is stable with respect to the Bohr-Wheeler condition (24) as we have previously discussed.

It is also worth mentioning that the result that  $\sigma_N/\sigma_C > 1$  for every nucleon density in our system can be explained as the result of the penetration of the relativistic electrons into the nucleus (see Refs. [49, 50] for details). This is allowed for configurations with sufficiently large sizes  $r_0 A^{1/3} > \hbar/(m_e c)$  or mass numbers  $A > \hbar^3/(r_0 m_e c)^3 \sim 10^7$ , where  $r_0 \approx 1.2$  fm. For systems with much larger mass numbers such as neutron stars,  $A_{NS} \sim 10^{57}$ , the penetration of electrons is such that they nearly neutralize the system and the electric field becomes appreciable only near the core surface [49, 50].

However, the transition layer could be unbound if the gravitational binding energy of the shell to the core is smaller

than its electrostatic energy. An approximate computation of the stability of the transition layer in the above sense can be found in Ref. [49], where it was shown within Newtonian gravity that the layer is gravitational bound provided the system has a number of baryons  $A \gtrsim 0.004(Z/A)^{1/2}(m_{Pl}/m_N)^3 \sim 10^{55}(Z/A)^{1/2}$  or a mass  $M = m_N A \gtrsim 0.01(Z/A)^{1/2}M_\odot$ , where  $m_N$  and  $m_{Pl} = (\hbar c/G)^{1/2}$  are the nucleon and Planck masses. It is clear that this stability requirement implies a lower limit for our globally neutral neutron stars. It would be interesting to perform a detailed calculation taking into account the effects of general relativity as well as of the magnetic field on the transition surface induced by rotation (see Ref. [52]) and the centrifugal potential acting on the shell. However, such calculation is out of the scope of this work and will be presented elsewhere.

#### IV. SURFACE TENSION IN PRESENCE OF THE CRUST

It was shown in Ref. [41] that the properties of the core-crust transition boundary layer depend on the nuclear parameters, especially on the nuclear surface tension, and on the density at the crust edge. The crust is composed of a nuclei lattice in a background of degenerate electrons, whose density at the edge of the crust is denoted here as  $n_e^{crust}$ . There are in addition free neutrons in the crust when the density of the crust,  $\rho_{crust}$ , is higher than the neutron-drip value  $\rho_{drip} \sim 4.3 \times 10^{11} \text{ g cm}^{-3}$  [44]. So when the density of the crust  $\rho_{crust}$  is smaller than the neutron-drip value, i.e.,  $\rho_{crust} < \rho_{drip}$ , we set the proton and neutron densities to zero in the outside region while the electron density must match the value  $n_e^{crust}$ , i.e.,  $n_{eo} = n_e^{crust}$ . In the cases when  $\rho_{crust} > \rho_{drip}$  both neutrons and electrons have to match their corresponding crust values at the end of the core-crust transition layer, i.e.,  $n_{eo} = n_e^{crust}$  and  $n_{no} = n_n^{crust}$ ,  $n_n^{crust}$  being the neutron density at the crust edge.

As shown by BBP [44] there is no proton-drip at any density of interest in these systems and therefore we keep zero as the outside proton density value. In order to set the matching density values for electrons and neutrons we use the relation of the free neutron and electron densities in Section 6 of the work by BBP [44]. At the neutron-drip point the electron Fermi momentum is around  $P_{eo}^F \approx 26 \text{ MeV}$  or  $P_{eo}^F/P_{eb}^F \approx 0.18$ , where  $P_{eo}^F$  is the electron Fermi momentum in the outside region and  $P_{eb}^F$  is the electron Fermi momentum in the bulk region.

The results of the dependence of the surface tension on the outside electron densities and the density of the crust are shown in Fig. 4. Here we also neglect the presence of the gravitational interaction, i.e.,  $(e^{\nu_{core}}, e^{-\lambda_{core}}) \rightarrow 1$ .

The results of Fig. 4 show that the Bohr-Wheeler condition (24) for the instability is reached at a crust density  $\rho_{crust}^{crit} \sim 1.2 \times 10^{14} \text{ g cm}^{-3}$ , so the system becomes unstable against fission when  $\rho_{crust} > \rho_{crust}^{crit}$ , imposing a physical upper limit to the density at the edge of the crust. It becomes interesting to include the binding effect of gravity and any other attractive contribution that strengthens the stability of the system, which will be analyzed elsewhere. It is interesting that this upper limit on the crust density implies a lower limit to the maxi-

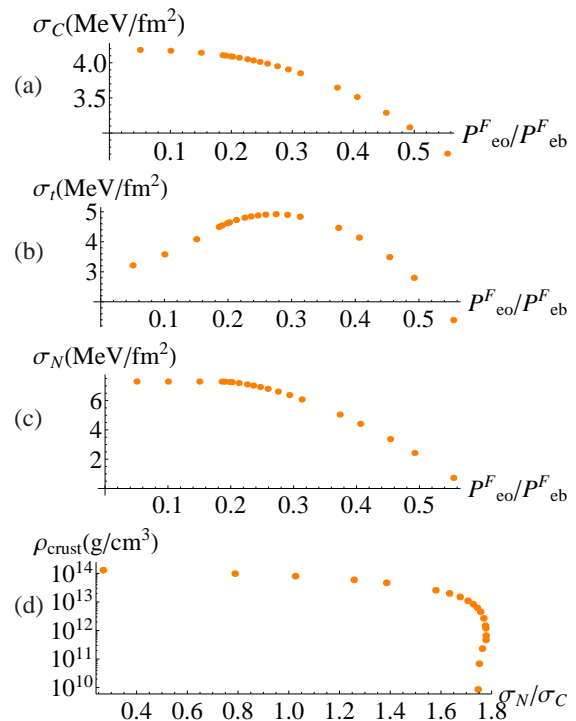


FIG. 4: (Color online) Dependence of the surface tension of the transition layer on the fermion densities in the outside region and the density of the crust. Here  $n_{bb} = n_{nucl}$  and  $(e^{\nu_{core}}, e^{-\lambda_{core}}) \rightarrow 1$ . (a) Surface tension for the electric field,  $\sigma_C$ . (b) The total surface tension  $\sigma_t$ . (c) The surface tension for nucleons,  $\sigma_N$ . (d) Ratio of the surface tension for nucleons and the surface tension for the electric field,  $\sigma_N/\sigma_C$ , with respect to the density of the crust  $\rho_{crust}$ . The neutron drip point  $\rho_{drip} \sim 4.3 \times 10^{11} \text{ g cm}^{-3}$  is around  $P_{eo}^F/P_{eb}^F \approx 0.18$ .

imum electric field in the core-crust transition region, limiting at the same time to approaching a state of quasilocal charge neutrality of the neutron star.

As shown in Fig. 4, the surface tension for the electric field decreases as increasing the electron number density in the outside region. The reason is that the increasing electron number density in the outside region [41] causes a decrease of the thickness of the interface and of the proton and electron density difference; i.e., the surface charge density decreases.

It is shown in Fig. 4 that the dependence of the surface tension for nucleons,  $\sigma_N$ , on the electron number density in the outside region is weak before the neutron drip point. The influence of electron density in the outside region on the surface structure of nucleons is small in this case. After the neutron drip point, the free neutrons in the outside region lower the surface tension significantly, as expected in the BBP phenomenological result [44]. In addition, as shown in Fig. 4, the total surface tension  $\sigma_t$  first increases and then decreases with increasing fermion densities in the outside region. This is due to the combination of the following two effects. (I) as shown in Table III, the contribution of electrons to the total surface tension is negative. For increasing electron density in the outside region, the effect of electrons on the surface tension becomes weaker. This increases the total surface tension.



(II) After the neutron drip point, the surface tension for nucleons  $\sigma_N$  is lowered significantly by the free neutrons in the outside region.

## V. EFFECTS OF THE GRAVITATIONAL INTERACTION ON THE SURFACE TENSION

We turn now to analyze the effects of the inclusion of the gravitational field on the surface tension of this transition layer. For the sake of simplicity, we make this analysis in the simplest case without a crust, considered in Section III.

As shown in Ref. [41], at the core radius (in this case the surface) of the neutron star, the metric functions are approximately the same as the Schwarzschild solution, so at the border of the star we have

$$e^{V_{core}} \approx e^{-\lambda_{core}} = 1 - \frac{2GM(R_{core})}{R_{core}}, \quad (42)$$

with  $M(R_{core})$  the mass of the star. The results of the solution of Eqs. (2)-(8) are shown in Fig. 5 for the case  $e^{\lambda_{core}} \approx e^{-V_{core}} = 1.5$ .

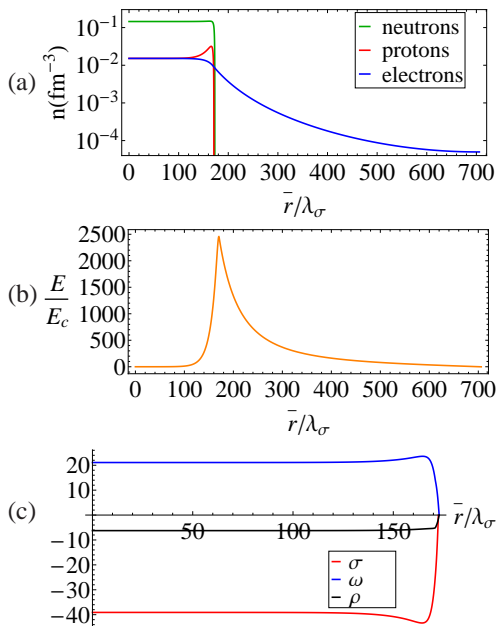


FIG. 5: (Color online) (a) Fermion density profiles in units of  $\text{fm}^{-3}$ . (b) Electric field in units of the critical field  $E_c$ . (c) Meson fields  $\sigma$ ,  $\omega$ , and  $\rho$  in units of MeV. Here we set  $e^{\lambda_{core}} \approx e^{-V_{core}} = 1.5$ ,  $n_{bb} = n_{nucl}$ , and  $n_{io} = 0$ .

Comparing to the results shown in Fig. 2, the fermion density and meson field profiles are similar to their counterparts in the case without the gravitational field. In Fig. 5 we see a larger proton density, a smaller neutron density, and a smaller size of the core-crust transition layer leading to a larger maximum of the electric field, comparing to Fig. 2.

Figure 6 shows the results of the dependence of the surface tension on the value of metric  $e^{\lambda_{core}}$ . As shown in Fig. 6, the

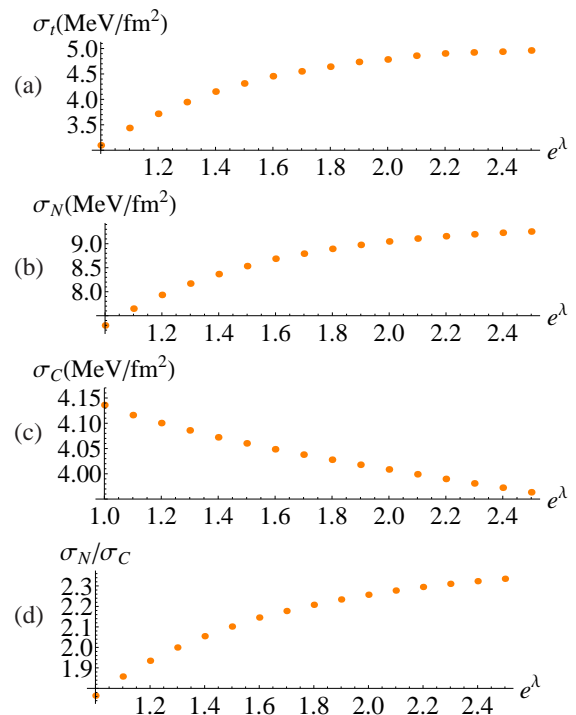


FIG. 6: (Color online) The dependence of the surface tension of the transition layer on the value of metric  $e^{\lambda_{core}}$ . (a) The total surface tension  $\sigma_r$ . (b) Surface tension for nucleons,  $\sigma_N$ . (c) Surface tension for the electric field,  $\sigma_C$ . (d) Ratio of the surface tension for nucleons and the surface tension for the electric field,  $\sigma_N/\sigma_C$ . We set here  $n_{bb} = n_{nucl}$  and  $n_{io} = 0$ .

total surface tension and the surface tension for nucleons increase as increasing the value of the metric  $e^{\lambda_{core}}$ . There are two effects which influence the characters of the total surface tension and the surface tension for nucleons. First, as we have seen the presence of gravitational field changes the fermion density and meson field profiles. Second, the difference between the proton density and the neutron density becomes smaller when the value of the metric  $e^{\lambda_{core}}$  increases, lowering the isospin asymmetry of the system. The combination of these two effects leads to the characters of the total surface tension and the surface tension for nucleons shown in Fig. 6. In addition, as shown in Fig. 6, the change of the value of the surface tension for the electric field when increasing the value of  $e^{\lambda_{core}}$  is small. That is due to the balance of the following two effects: (I) the electric field in the surface region becomes larger (see Fig. 5); (II) the thickness of the surface becomes smaller, and then the Coulomb energy distributes in a smaller region. It can be also checked from Fig. 5 how in the limit  $e^{\lambda_{core}} \rightarrow 1$  all quantities tend to the values found in Sec. III in the flat case.

## VI. SUMMARY AND DISCUSSION

Taking into account strong, weak, electromagnetic, and gravitational interactions, and fulfilling the global charge neu-

trality of the system, a transition layer will happen between the core and crust of neutron stars [41]. This is different from the results from traditional TOV equations imposing local charge neutrality. This core-crust transition layer happens at the saturation density of nuclear matter. In this article, using RMFT together with the Thomas-Fermi approximation, we study the surface properties of this transition layer. In particular, we computed the surface tension and Coulomb energy of the transition shell and analyzed the role of each fermion component and meson fields in the determination of the properties of this core-crust transition layer.

Since the length scale of the core-crust transition layer ( $\sim \lambda_e$ ) is much smaller than the radius of neutron stars and the electron density is nearly equal to the proton density in the bulk hadronic phase of neutron star cores, we applied the semi-infinite matter model as an approximation to construct the surface tension for this core-crust transition layer, following the method of BBP in Ref. [44]. We first presented the studies of this transition layer neglecting the presence of the gravitational interaction. We calculated the surface tension and the Coulomb energy for the transition layer of this system for different baryon number densities near the nuclear saturation density. The results show that the total surface tension as well as the surface tension for the electric field and the surface tension for nucleons are proportional to some power-law function of the baryon number density in the bulk region; see Eqs. (37)-(39). The difference between the surface energy of this neutron star matter and the phenomenological results [44] in nuclear physics has been analyzed. We also studied the surface structure for different fermion densities in the outside region, namely for different densities of the neutron star crust.

We also presented the analysis of the influence the gravitational field and on the structure of the transition layer and the surface tension. The results show that the fermion density and meson field profiles are similar to the case without the presence of gravitational field, although some quantitative differences appear. We show that the total surface tension and the surface tension for nucleons increase with increasing value of the metric function  $e^{\lambda_{core}}$ .

We studied the instability against Bohr-Wheeler surface deformation for all the systems. We find that the instability sets in at a critical density of the crust  $\rho_{crust}^{crit} \sim 1.2 \times 10^{14} \text{ g cm}^{-3}$ . This implies a lower limit to the maximum electric field of the core-crust transition region and makes inaccessible a state of quasilocal charge neutrality for the neutron star, which will in principle be reached when the limit  $\rho_{crust} = \rho_{core} \approx \rho_{nucl}$  is approached.

The results of this work open the way to more general studies relevant for the analysis of the stability of neutron stars and the core-crust transition surface. Some of the effects that need to be addressed for the stability of the shell include gravitational binding, centrifugal repulsion, magnetic field induced by rotating electric field and hence magnetic dipole-dipole interactions. It would be interesting to perform a similar analysis for the case of strange stars both bare and in the presence of an outer crust.

It is also important to mention that surface effects and boundary layers are contained in the widely discussed nuclear

pasta phases (see, e.g., Refs. [15–18], and references therein) expected in the low-density nuclear matter composing the inner crust of neutron stars. Those configurations also fulfill the condition of global charge neutrality. However, in there the condition of global charge neutrality is only imposed in the pasta phase while keeping the condition of local charge neutrality in the rest of the configuration, e.g., in the core of the neutron star. In contrast, in our model, the global charge neutrality is fulfilled in the whole configuration, which leads to the phenomenon of gravito-polarization in the core of the neutron star. Along this line, it would be interesting to study the differences of these two scenarios and to establish which is the configuration of minimum energy and therefore realized in nature. This is a very interesting question which deserves a detailed and deep analysis; however, it is out of the scope of the present work and we therefore leave it for a future publication.

To end, it is interesting to briefly discuss some of the observables which could shed light into the structure of the neutron star and therefore to probe the underlying theory.

On one hand, there might be some effects coming from the microscopic structure. One possibility could be some electromagnetic processes due to the strong electric field in the core-crust interface, such as the annihilation line of  $e^-e^+$  to two photons. These  $e^-e^+$  pairs can be produced by neutron star perturbations. However, this effect could be difficult to observe with the current instrumentation; we are planning to analyze in detail this interesting problem elsewhere.

On the other hand, as we have pointed out, from the macroscopic structure point of view the new structure of the neutron star leads to different radii due to the different size of the crust. This necessarily leads to the possibility of probing the theory of neutron stars and in particular the physics of the core-crust transition from reliable observations of their masses and radii. Such measurements can come for instance from observations of the thermal evolution of accreting and isolated neutron stars. In particular, observations of the cooling of the neutron star during its thermal relaxation phase ( $t \lesssim 50 \text{ yr}$  after birth), where the core and the crust are thermally decoupled, carry crucial information on the core-crust transition density and therefore on the crust mass and size [53].

If we move on to the last stages of the life of a neutron star, it is clear that the electromagnetic structure of the neutron star is particularly relevant for the process of its gravitational collapse. A core endowed with electromagnetic structure leads to signatures and energetics markedly different from the ones of a core endowed uniquely of gravitational interactions *à la* Oppenheimer and Snyder [54]; see, e.g., Refs. [55–58]. As pointed out recently [59, 60], in these cores there are electric processes that might lead to a vast  $e^-e^+$  production in the process of collapse to a black hole.

## Acknowledgement

Yuan-Bin Wu is supported by the Erasmus Mundus Joint Doctorate Program by Grant Number 2011-1640 from the EACEA of the European Commission.

- 
- [1] H. P. Duerr, *Phys. Rev.* 103, 469 (1956).
- [2] L. D. Miller and A. E. S. Green, *Phys. Rev. C* 5, 241 (1972).
- [3] J. D. Walecka, *Ann. Phys.* 83, 491 (1974).
- [4] J. Boguta and J. Rafelski, *Phys. Lett. B* 71, 22 (1977).
- [5] J. Boguta and A. R. Bodmer, *Nucl. Phys. A* 292, 413 (1977).
- [6] T. D. Lee and G. C. Wick, *Phys. Rev. D* 9, 2291 (1974).
- [7] T. D. Lee, *Rev. Mod. Phys.* 47, 267 (1975).
- [8] T. D. Lee, M. Margulies, *Phys. Rev. D* 11, 1591 (1975).
- [9] J. Boguta and H. Stocker, *Phys. Lett. B* 120, 289 (1983).
- [10] J. Boguta and S. A. Moszkowski, *Nucl. Phys. A* 403, 445 (1983).
- [11] J. Boguta, *Nucl. Phys. A* 501, 637 (1989).
- [12] B. D. Serot, *Rept. Prog. Phys.* 55, 1855 (1992).
- [13] P. Ring, *Prog. Part. Nucl. Phys.* 37, 193 (1996).
- [14] M. Bender, P.-H. Heenen, and P.-G. Reinhard, *Rev. Mod. Phys.* 75, 121 (2003).
- [15] T. Maruyama, T. Tatsumi, D. N. Voskresensky, T. Tanigawa, and S. Chiba, *Phys. Rev. C* 72, 015802 (2005).
- [16] S. S. Avancini, D. P. Menezes, M. D. Alloy, J. R. Marinelli, M. M. W. Moraes, and C. Providência, *Phys. Rev. C* 78, 015802 (2008).
- [17] M. Okamoto, T. Maruyama, K. Yabana, and T. Tatsumi, *Phys. Lett. B* 713, 284 (2012).
- [18] F. Grill, C. Providência, and S. S. Avancini, *Phys. Rev. C* 85, 055808 (2012).
- [19] R. J. Furnstahl, B. D. Serot, and H. B. Tang, *Nucl. Phys. A* 598, 539 (1996).
- [20] R. J. Furnstahl, B. D. Serot, and H. B. Tang, *Nucl. Phys. A* 615, 441 (1997); A640, 505 (1998).
- [21] B. D. Serot and J. D. Walecka, *Int. J. Mod. Phys. E* 06, 515 (1997).
- [22] M. Brack, C. Guet, and H.-B. Håkansson, *Phys. Rep.* 123, 275 (1985).
- [23] M. M. Sharma, S. A. Moszkowski, and P. Ring, *Phys. Rev. C* 44, 2493 (1991).
- [24] D. Von-Eiff, J. M. Pearson, W. Stocker, and M. K. Weigel, *Phys. Lett. B* 324, 279 (1994).
- [25] D. Von-Eiff, W. Stocker, and M. K. Weigel, *Phys. Rev. C* 50, 1436 (1994).
- [26] D. Von-Eiff, H. Freyer, W. Stocker, and M. K. Weigel, *Phys. Lett. B* 344, 11 (1995).
- [27] M. Centelles, M. Del Estal, and X. Viñas, *Nucl. Phys. A* 635, 193 (1998).
- [28] M. Del Estal, M. Centelles, and X. Viñas, *Nucl. Phys. A* 650, 443 (1999).
- [29] S. K. Patra, M. Centelles, X. Viñas, and M. Del Estal, *Phys. Rev. C* 65, 044304 (2002).
- [30] P. Danielewicz and J. Lee, *Nucl. Phys. A* 818, 36 (2009).
- [31] N. K. Glendenning, *Phys. Rev. D* 46, 1274 (1992).
- [32] N. K. Glendenning, *Phys. Rep.* 342, 393 (2001).
- [33] N. K. Glendenning and J. Schaffner-Bielich, *Phys. Rev. C* 60, 025803 (1999).
- [34] M. B. Christiansen, N. K. Glendenning, and J. Schaffner-Bielich, *Phys. Rev. C* 62, 025804 (2000).
- [35] M. Alford, K. Rajagopal, S. Reddy, and F. Wilczek, *Phys. Rev. D* 64, 074017 (2001).
- [36] D. G. Ravenhall, C. J. Pethick, and J. R. Wilson, *Phys. Rev. Lett.* 50, 2066 (1983).
- [37] M. Rotondo, J. A. Rueda, R. Ruffini, and S.-S. Xue, *Phys. Lett. B* 701, 667 (2011).
- [38] J. A. Rueda, R. Ruffini, and S.-S. Xue, *Nucl. Phys. A* 872, 286 (2011).
- [39] R. C. Tolman, *Phys. Rev.* 55, 364 (1939).
- [40] J. R. Oppenheimer and G. Volkoff, *Phys. Rev.* 55, 374 (1939).
- [41] R. Belvedere, D. Pugliese, J. A. Rueda, R. Ruffini, and S.-S. Xue, *Nucl. Phys. A* 883, 1 (2012).
- [42] P. Haensel, A. Y. Potekhin, and D. G. Yakovlev, *Neutron Stars 1: Equation of State and Structure*, Springer-Verlag, New York, 2007.
- [43] N. Bohr and J. A. Wheeler, *Phys. Rev.* 56, 426 (1939).
- [44] G. Baym, H. A. Bethe, and C. J. Pethick, *Nucl. Phys. A* 175, 225 (1971).
- [45] J. Boguta, *Phys. Lett. B* 106, 255 (1981).
- [46] G. A. Lalazissis, J. König, and P. Ring, *Phys. Rev. C* 55, 540 (1997).
- [47] T. D. Lee and Y. Pang, *Phys. Rev. D* 35, 3678 (1987).
- [48] B. Cameron, *Eur. J. Phys.* 30, 763 (2009).
- [49] M. Rotondo, R. Ruffini, S.-S. Xue, and V. Popov, *Int. J. Mod. Phys. D* 20, 1995 (2011).
- [50] M. Rotondo, J. A. Rueda, R. Ruffini, and S.-S. Xue, *Phys. Rev. C* 83, 045805 (2011).
- [51] P.-G. De Gennes, F. Brochard-Wyart, and D. Quéré, *Capillary and Wetting Phenomena: Drops, Bubbles, Pearls, Waves*, Springer, New York, 2003.
- [52] K. Boshkayev, M. Rotondo, and R. Ruffini, *Int. J. Mod. Phys. Conf. S.* 12, 58 (2012).
- [53] S. M. de Carvalho, R. Negreiros, J. A. Rueda, and R. Ruffini, to be submitted.
- [54] J. R. Oppenheimer and H. Snyder, *Phys. Rev.* 56, 455 (1939).
- [55] R. Ruffini, L. Vitagliano and S.-S. Xue, *Phys. Lett. B* 573, 33 (2003).
- [56] R. Ruffini, L. Vitagliano and S.-S. Xue, *Phys. Lett. B* 559, 12 (2003).
- [57] R. Ruffini and S.-S. Xue, *AIP Conf. Proc.* 1059, 72 (2008).
- [58] R. Ruffini, G. V. Vereshchagin and S.-S. Xue, *Phys. Rep.* 487, 1 (2010).
- [59] W.-B. Han, R. Ruffini, and S.-S. Xue, *Phys. Rev. D* 86, 084004 (2012).
- [60] R. Ruffini and S.-S. Xue, *Phys. Lett. A* 377, 2450 (2013).